POLITECNICO DI TORINO
Repository ISTITUZIONALE

Advanced Circuital Model for e-Drive Simulation, Including Harmonic Effects and Fault Scenarios

(Article begins on next page)

18 September 2024

Advanced Circuital Model for e-Drive Simulation, Including Harmonic Effects and Fault Scenarios

Andrei Bojoi[1], Simone Ferrari[1], Paolo Pescetto[1], Gianmario Pellegrino[1]

[1] Politecnico di Torino, Department of Energy *Galileo Ferraris*, Italy

Corresponding author: Andrei Bojoi, andrei.bojoi@polito.it
Speaker: Andrei Bojoi, andrei.bojoi@polito.it

Abstract

The paper presents an advanced circuital model of e-drive for control firmware development and real-time simulation purposes, compatible with Simulink and PLECS environments. The model accounts for PWM voltage supply, magnetic saturation, iron losses and space harmonic fields in the e-motor, and covers both healthy and faulty scenarios. The use of advanced $dq\theta$ flux maps allows for accurate simulation of torque ripple and back-EMF undulation. The proposed model is experimentally validated on a traction PMSM and can be automatically generated within the SyR-e open-source design platform.

1 Introduction

The design study of an e-Motor normally involves two main steps: (1) the electromagnetic, mechanical and thermal design using optimization procedures based on Finite Element Analysis (FEA) and (2) the simulation of the e-Drive for motor control design and calibration purposes, using accurate models for both e-motor and inverter. In both stages, dedicated softwares were developed for semi-automated motor design and performance evaluation [1], [2]. Among these, the most comprehensive ones cover different types of motor drives, including Permanent Magnet Synchronous Motors (PMSMs) and Synchronous Reluctance (SyR) motors [3].

Dealing with the motor simulation for control design purposes, an accurate representation of the machine should include its space harmonics, which may affect the control accuracy and stability, as well as iron and PM losses effects. To cover these aspects, a number of FEA-coupled motor models were developed [4], [5], obtaining high accuracy of the drive simulation at the cost of high computational burden, often resulting in not acceptable execution time. For this reason, this paper focuses on the circuital models of the Synchronous Machines (SM), capable of representing space harmonics and iron and PM loss effects with no need of time consuming FEA co-simulation.

The two most used approaches for simulating an electromagnetic system are the analytical and circuital models. In the first ones, the motor equations are implemented by using signal blocks, while in the latter one physical libraries are adopted, such as resistors, inductors, current/voltage sources and so on. In this work, the latter approach is preferred as it permits to better represent the machine under faulty conditions, such as open or short circuit, either symmetrical or not.

Nowadays, the most widely used softwares for motor drives simulation are Matlab-Simulink and PLECS, both including several motor models. In the Simulink library, two blocks are considered: the *Synchronous Reluctance Machine* [6] and the *FEM Parametrized PMSM* [7]. Starting from the current vectors components i_d, i_q, the magnetic saturation and cross-coupling effects are described by means of apparent inductance matrices $\boldsymbol{L_{dq}}(\boldsymbol{i_{dq}})$ in the former block and flux linkage matrices $\boldsymbol{\lambda}_{dq}(\boldsymbol{i_{dq}},\theta)$ in the latter block, where θ is the electrical angle. Both models can include the iron losses effects, implemented stator and rotor loss tables $\boldsymbol{P_s}(\boldsymbol{i_{dq}},\omega)$ and $\boldsymbol{P_r}(\boldsymbol{i_{dq}},\omega)$, function of the current vector and the electrical speed ω. However, the Simulink environment does not provide an unified model covering all the SM types, to be adopted for automated design tools [1]. Moreover, the PM losses are not taken into account and the space harmonics can be represented only if adopting the *FEM Parametrized*
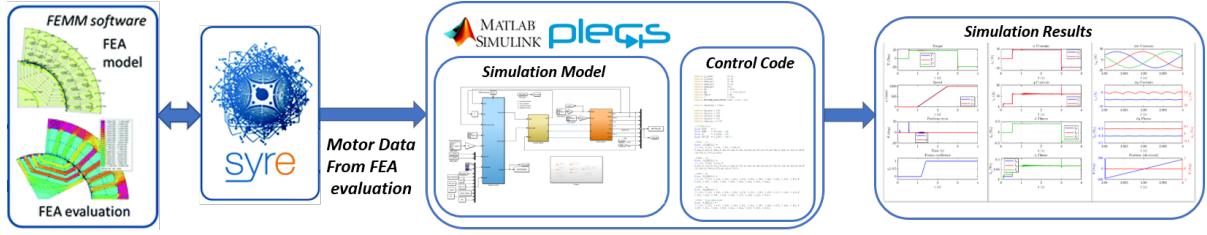
Fig. 1: Operating principle of syreDrive.

PMSM, but this considerably increases the execution time of the simulation.

A different approach is adopted by the PLECS library, which includes two blocks called *Non-excited SM* [8] and *Permanent-Magnet SM* [9]. The former block is a series RLE circuit using the Voltage Behind Reactance (VBR) modeling approach [10], where the magnetic saturation is implemented by means of flux linkage $\boldsymbol{\lambda}_{dq}(\boldsymbol{i}_{dq})$ and incremental inductance $\boldsymbol{l}_{dq}(\boldsymbol{i}_{dq})$ lookup tables (LUTs). The latter block may be configured as two different solutions: the VBR model (neglecting mutual inductance and assuming constant L_d, L_q inductances) and the *Rotor Reference Frame* model, consisting of two controlled current sources for phases a and c. The flux linkage vector $\boldsymbol{\lambda}_{dq}$ is retrieved from phase voltage integration. The ratio between the obtained $\boldsymbol{\lambda}_{dq}$ vector components and the respective inductances L_d, L_q provides the i_d, i_q current components, subsequently transformed in the abc axis. The main drawbacks of these models are the impossibility of representing the iron losses, the space harmonics and, for the *Permanent-Magnet SM*, the magnetic saturation.

The circuital representation using current generators was also used in [11], where a switched reluctance machine is modeled in Simulink as four controlled current generators, one per each phase. The flux linkages $\boldsymbol{\lambda}_{abc}$ are obtained from integration of back-EMF voltages, computed from the motor phase voltage $\boldsymbol{v}_{abc}$ and its resistance voltage drop. The motor torque and current, feeding the controlled current generators, are given by dedicated LUTs, based on the flux linkages and electrical rotor position.

As described above, all the available PLECS and Simulink models have several limitations. This paper presents an unified circuital e-drive model, suitable for PMSMs and SyR machines, compatible with both Simulink and PLECS environments. The model accounts for PWM voltage supply, magnetic saturation, iron and PM losses and harmonic fields

in the e-motor, without significant impact on the computational burden and execution time. In addition, the circuital model permits simulating the drive under healthy and faulty conditions.

The proposed work is a contribution to syreDrive [1], a tool for e-drives simulation included in the e-motor design software SyR-e, whose operating principle is presented in Fig.1. Given the motor data, either computed through FEA or experimentally measured, syreDrive generates a self-calibrated e-drive model in Simulink or PLECS, permitting to choose between different control strategies, including several sensorless controls.

2 Motor model and magnetic model representation

A SM can be modelled in 3-phase, stationary or rotating reference frames, respectively called abc, $\alpha\beta$ and dq. The rotational and the Clark transformation matrices convert every electromagnetic quantity between the different reference frames:

$$\boldsymbol{A}(\theta) = \begin{bmatrix} cos(\theta) & sin(\theta) \\ -sin(\theta) & cos(\theta) \end{bmatrix} \quad (1)$$

$$\boldsymbol{T} = \begin{bmatrix} \frac{2}{3} & -\frac{1}{3} & -\frac{1}{3} \\ 0 & \frac{\sqrt{3}}{3} & -\frac{\sqrt{3}}{3} \\ \frac{1}{3} & \frac{1}{3} & \frac{1}{3} \end{bmatrix} \quad (2)$$

The stator voltage vector $\boldsymbol{v}_{dq}$ of a SM is given by:

$$\boldsymbol{v}_{dq} = R_s \boldsymbol{i}_{dq} + \frac{d\boldsymbol{\lambda}_{dq}}{dt} + \omega \mathbf{J} \boldsymbol{\lambda}_{dq} \quad (3)$$

where $\mathbf{J} = \begin{bmatrix} 0 & -1 \\ 1 & 0 \end{bmatrix}$ is the imaginary unit expressed in matrix form, $\boldsymbol{x}_{dq} = [x_d, \ x_q]^T$ is a generic vector in dq coordinates and R_s is the stator resistance. Independently from the circuital model approach, the identity of an e-motor is represented by its magnetic model, or flux maps, i.e. the dq flux linkages $\boldsymbol{\lambda}_{dq}$ as a function of dq stator currents $\boldsymbol{i}_{dq}$:

$$\boldsymbol{\lambda}_{dq} = \boldsymbol{\lambda}_{dq} \left(\boldsymbol{i}_{dq} \right) \quad (4)$$
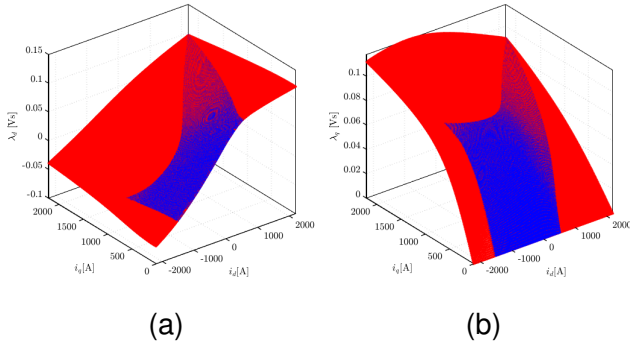
Fig. 2: Direct (red) and inverse (blue) magnetic model. (a) $\lambda_d(i_d, i_q)$ and (b) $\lambda_q(i_d, i_q)$.

The flux maps are normally stored in form of Look-Up-Tables (LUTs). Two types of magnetic models can be considered [12]: the dq or the $dq\theta$ model. The LUTs of dq flux maps, labeled $\boldsymbol{\lambda}_{dq}(\boldsymbol{i}_{dq})$, represent the fundamental saturation model, averaged over one electrical or mechanical period. On the other side, the $dq\theta$ flux map $\boldsymbol{\lambda}_{dq}(\boldsymbol{i}_{dq}, \theta)$ includes the effects of rotor position on torque and flux linkages components, i.e. torque ripple and back-EMF undulation, thus modeling also the space harmonics of the machine. The iron and PM losses can be described by means LUTs as well [13], depending on the $\boldsymbol{i}_{dq}$ current components and electrical speed ω. In SyR-e, these maps are FEA evaluated at a reference electrical speed ω_0, and then rescaled according to the operating speed.

Additionally, the magnetic models can be distinguished between direct and inverse models. Both of them can be associated to the dq or $dq\theta$ approach. Either if obtained by FEA softwares or measured by experiments, the flux maps are normally evaluated in their direct form, i.e. $\boldsymbol{\lambda}_{dq}(\boldsymbol{i}_{dq})$, computed in a regular grid of points on the (i_d, i_q) current plane. Because of the magnetic saturation, such regular current domain does not correspond to a regular area in the flux plane (λ_d, λ_q). For the simulation models requiring the $\boldsymbol{i}_{dq}(\boldsymbol{\lambda}_{dq})$ LUT (inverse magnetic model), the direct flux maps must be numerically reversed, often with significant loss in the covered domain, thus representing the machine in a smaller range of operating points. An example is given in Fig. 2, where the direct and inverse flux maps of a PMSM are reported in red and blue respectively, for the d and q axes. The reduction in the current/flux domain due to LUTs reversal is clearly visible.

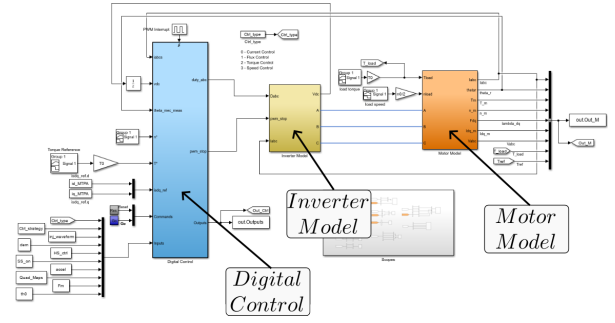To conclude, the simulation models adopting the di-

Fig. 3: Simulink e-Drive simulation model.

rect flux maps are preferred over the ones requiring the maps inversion.

3 Circuital modelling approaches

Fig. 3 reports the complete e-drive Simulink model, as implemented in syreDrive. The PLECS counterpart is formally equivalent, and not reported here for brevity.

The model includes three main blocks: the circuital inverter and motor models, and the digital control. This is implemented as an S-function using an ANSI C-script, configurable in torque or speed control. The torque control can be implemented with different solutions, such Field-Oriented-Control (FOC) or Direct-Flux-Vector-Control (DFVC). SyreDrive also includes several options for position sensorless control.

Dealing with the motor model, this paper considers two alternative circuital approaches [14], for comparison purposes:

1. Voltage Behind Reactance (VBR) model.

2. Controlled Current Generators (CCG) model.

The two models, described hereafter, were inspired by the *Non-Excited SM* PLECS component and by the Simulink model in [11] respectively, introduced in Section 1. Both VBR and CCG models can embed either a dq or $dq\theta$ magnetic model.

3.1 Motor model: voltage behind reactance

For the VBR approach, the Simulink and PLECS circuital models are reported in Fig. 4a and 4b, while the block diagram of the operating principle is reported in Fig. 4c. The e-motor is represented as an RLE circuit, with the coupled variable inductors accounting for self- and cross- magnetic saturation. The controlled voltage generators correspond to the motor back-EMFs, analytically computed by the
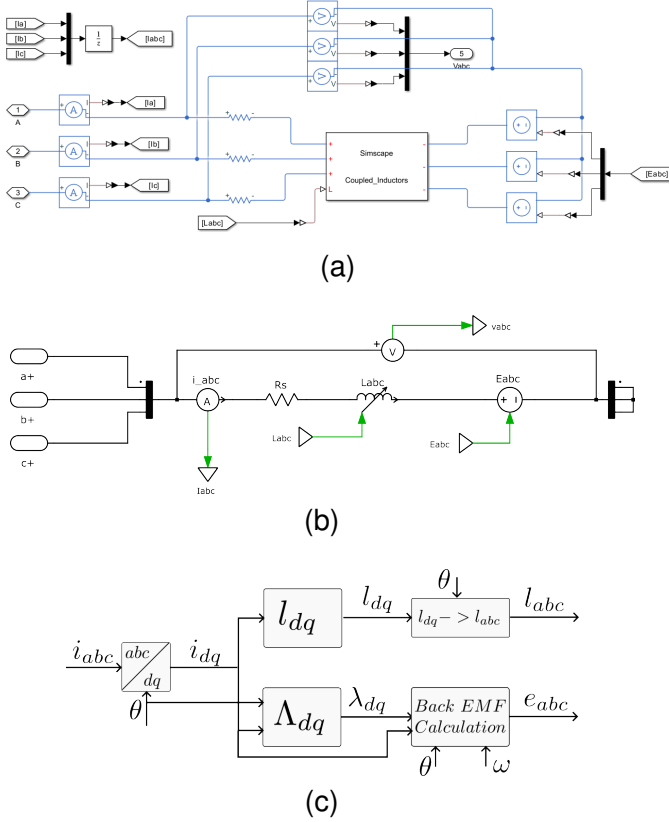
(a)

(b)

(c)

Fig. 4: VBR model: Simulink (a) and PLECS (b) circuital model and associated block diagram (c).

Fig. 5: Direct flux maps: $\lambda_d(\boldsymbol{i}_{dq})$ (a) and $\lambda_q(\boldsymbol{i}_{dq})$ (b).

model. If the PLECS library already included the *Variable Inductor* component for the three-phase coupled inductances, an equivalent component was custom designed in Simulink, using the Simscape language.

The VBR model requires both the direct flux maps ($\boldsymbol{\Lambda}_{dq}(\boldsymbol{i}_{dq})$ for the dq model, reported in Fig. 5a. 5b, or $\boldsymbol{\Lambda}_{dq}(\boldsymbol{i}_{dq}, \theta)$ for the the $dq\theta$ model) and the incremental inductance maps. These can be numerically retrieved from the flux maps. In particular, three inductance LUTs are required: $l_d(\boldsymbol{i}_{dq})$, $l_q(\boldsymbol{i}_{dq})$ and $\boldsymbol{l}_{dq}(\boldsymbol{i}_{dq})$. The output of these inductance LUTs are organized the $\boldsymbol{l}_{dq} = \begin{bmatrix} l_d & l_{dq} \\ l_{qd} & l_q \end{bmatrix}$ matrix.

If the magnetic saturation is conveniently expressed in the dq frame, the motor circuital model must be implemented in the 3-phase abc frame. Therefore, the $\boldsymbol{l}_{dq}$ matrix is reported in abc axes through Clarke and rotation transformations:

$$\boldsymbol{l}_{\alpha\beta} = \boldsymbol{A}(-\theta) \cdot \boldsymbol{l}_{dq} \cdot \boldsymbol{A}(\theta) \tag{5}$$

$$\boldsymbol{l}_{abc} = \boldsymbol{T}^{-1} \cdot \boldsymbol{l}_{\alpha\beta} \cdot \boldsymbol{T} \tag{6}$$

The 9 elements of the $3x3$ matrix $\boldsymbol{l}_{abc}$ are provided

to the *coupled inductors* component, while the back-EMFs are obtained as:

$$\boldsymbol{e}_{dq} = \boldsymbol{l}_{dq}(-\omega)\boldsymbol{J}\boldsymbol{i}_{dq} + \boldsymbol{J}\omega\boldsymbol{\lambda}_{dq} \tag{7}$$

The $\boldsymbol{e}_{dq}$ vector is then reported in abc frame and fed to the controlled voltage generators.

3.2 Motor model: controlled current generator model

Dealing with the CCG circuital models, the Simulink and PLECS implementations are reported in Fig. 6a and 6b, while its equivalent block diagram is reported in Fig.6c.

In both the simulation environments, the circuital model includes three controlled current sources, imposing the three phase motor currents $\boldsymbol{i}_{abc}$. The current sources are in series with the phase resistances R_s. Large resistors are added in parallel for aiding the convergence of the numerical solver. The voltage drops across the current generators correspond to the phase back-EMFs.

The state variables of the model are the flux linkages, obtained by integration of the measured back-EMFs in $\alpha\beta0$ axes. The dq flux linkages $\boldsymbol{\lambda}_{dq}$ are the inputs to the LUTs of the inverse magnetic model (inverse flux maps) $\boldsymbol{\Lambda}_{dq}^{-1}$, i.e the $\boldsymbol{i}_{dq}(\boldsymbol{\lambda}_{dq})$, as reported in Fig.7a-7b, or $\boldsymbol{i}_{dq}(\boldsymbol{\lambda}_{dq}, \theta)$. As detailed in Section 2, the flux maps inversion reduces the available domain of LUTs. The limits can be easily corrected with FEA modeling, but not with experimental flux maps obtained from motor testing [15]. The $\boldsymbol{i}_{dq}$ vector is output from the inverse magnetic model. The homopolar current i_0 is also considered, obtained from the homopolar flux λ_0 and the leakage inductance L_σ. This permits to include the modeling of asymmetrical faulty conditions. Finally, the $\boldsymbol{i}_{dq0}$ vector is transformed in abc axes through rotation and Clarke transformation and fed to the controlled current generators.
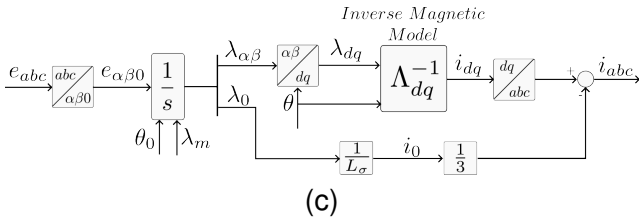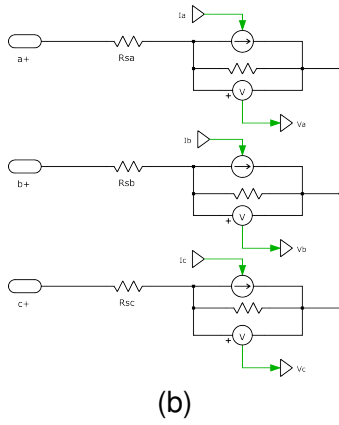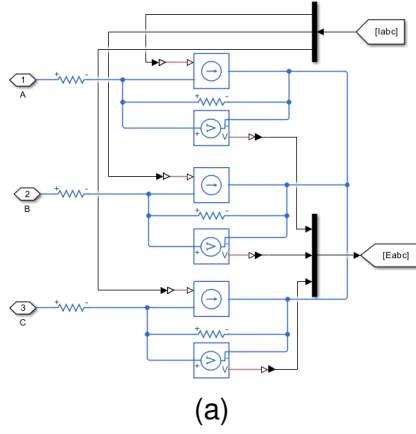
(a)

(b)

(c)

Fig. 6: CCG model: Simulink (a) and PLECS (b) model and associated block diagram (c).

3.3 Inverter Circuital Model

In both Simulink and PLECS environment, the inverter is implemented with a circuital model, as reported in Fig. 8a and 8b. In both cases, the model includes the modulator block, which can be alternatively set as *instantaneous* or *time average*. In the former configuration, a PWM modulation is implemented, and the inverter is fed with the 6 switching functions, accounting for the dead-time. In the latter case, the simulation model directly imposes the average inverter voltage over the PWM period. In this case, the motor is fed with a continuous voltage, neglecting the switching phenomena, and the dead time effects are taken into account as a variable voltage drop depending on the current direction. Despite the commutations are disabled,
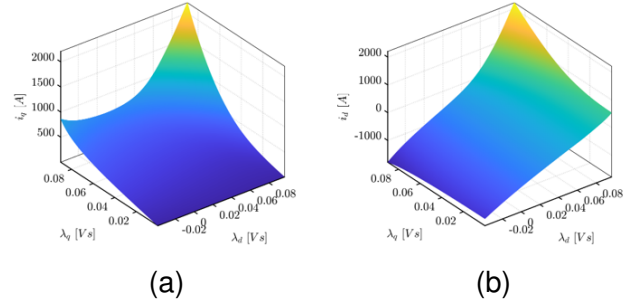

(a)   (b)

Fig. 7: Inverse flux maps: $i_d(\boldsymbol{\lambda}_{dq})$ (a) and $i_q(\boldsymbol{\lambda}_{dq})$ (b).

the PLECS VSI component still requires the input duty cycles of the six switches. The commands for the upper switches are computed as

$$g_k = d_k - sgn(i_k) \cdot dT \cdot f_{sw} \qquad k = a, b, c \quad (8)$$

where dT is the dead time and f_{sw} the switching frequency. The commands for the lower switches are given by the logical negation of (8).
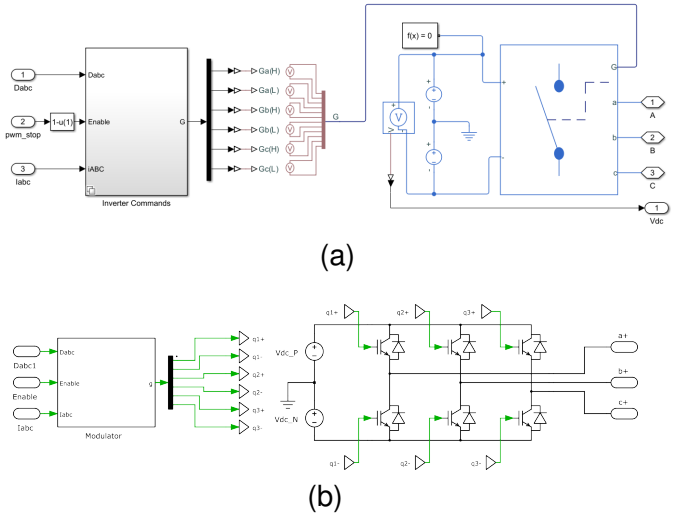

(a)

(b)

Fig. 8: Inverter circuital implementation: Simulink (a) and PLECS (b).

In PLECS, the inverter component configuration is called *Sub-cycle average* [16], able to run in fixed-step real-time simulation.

4 Simulation results

The proposed eDrive model was tested both in Simulink and Plecs simulation environments, with either CCG or VBR approaches, for comparison purposes.

4.1 Execution time comparison

The e-drive model was run for $1s$ of simulation time, on a laptop equipped with Intel(R) Core(TM) i7-

10750H CPU @ 2.60GHz. All possible configurations (dq or $dq\theta$ magnetic model, CCG or VBR representation, Simulink or PLECS environment, instantaneous or time average inverter) were covered. For each case, the simulaiton was repeated 5 times, and the average execution time is reported in Fig. 9. Both for the PLECS and Simulink simulations a variable step solver was used, with the same tolerance ($1e - 3$) and maximum step size ($2~\mu s$).
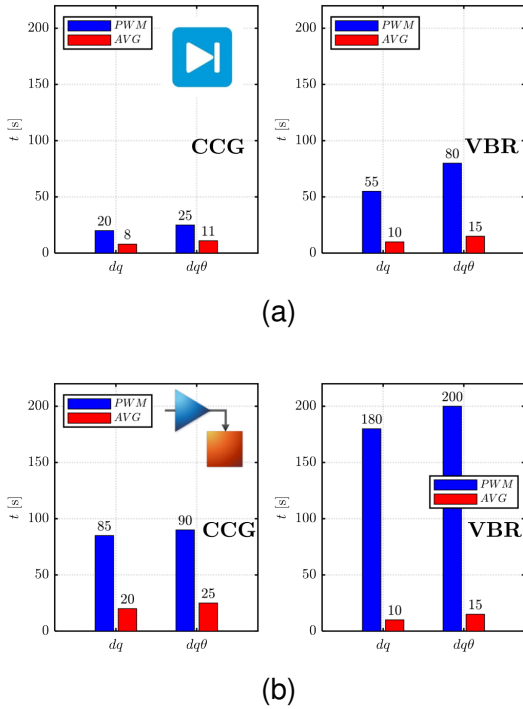

(a)

(b)

Fig. 9: Execution time for 1s simulation: (a) PLECS models and (b) Simulink models.

The comparison demonstrates that the PLECS solver is considerably faster than the Simulink one, and that the VBR approach is much slower than the CCG one. As expected, the dq model is faster than the $dq\theta$ one, because of the higher computational effort related to the 3D LUTs instead of 2D ones. Because of the much faster execution time, the CCG model is selected to be integrated in syreDrive, and further developed to include the iron and PM losses.

4.2 Comparison between dq and $dq\theta$ models

The dq and $dq\theta$ models were tested for a 430 Nm traction PMSM, having a base speed of 4200 rpm and a maximum speed of 18000 rpm. The simulation results for a full torque reversal at a constant speed of 2000 rpm are compared in Fig. 10.
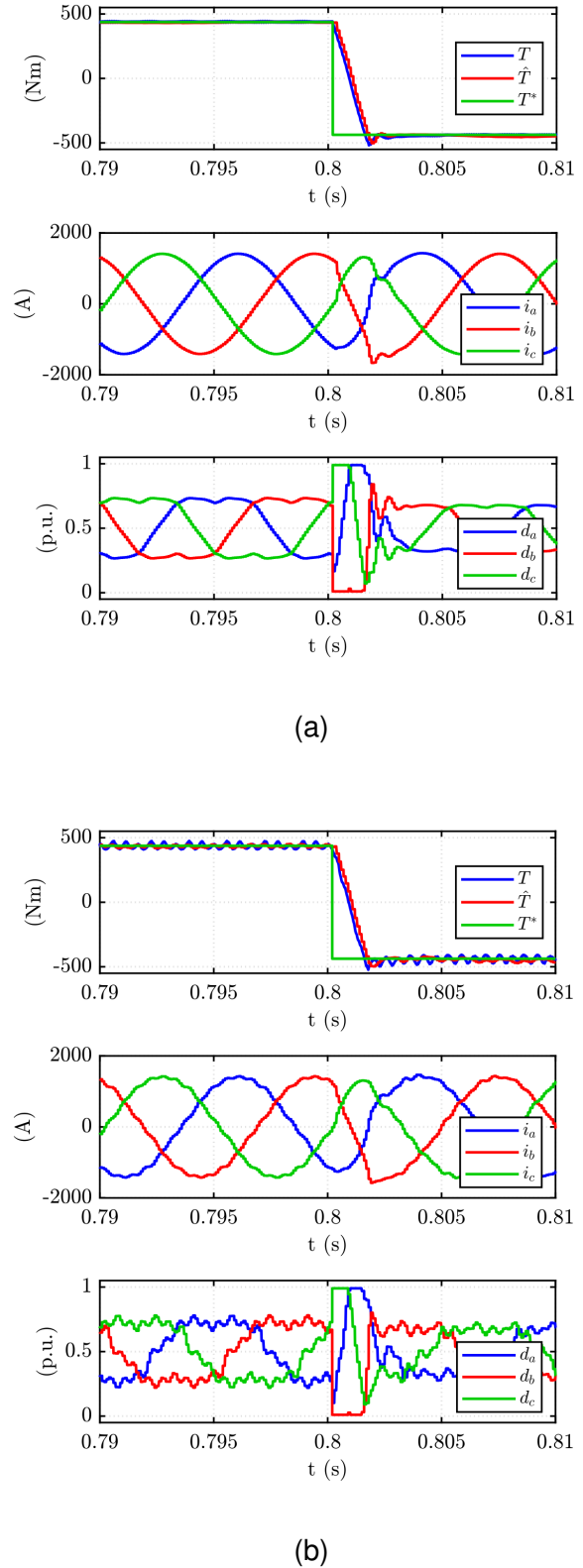

(a)

(b)

Fig. 10: Simulated torque, current and duty cycles under torque reversal at constant speed. (a) dq model; (b) $dq\theta$ model.

Despite its higher computational burden, it is evident the $dq\theta$ model includes torque and back-
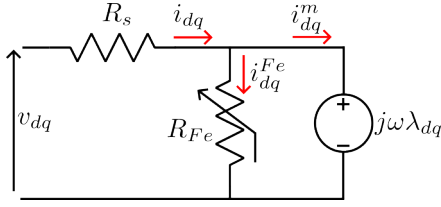
Fig. 11: Equivalent circuit in dq axes, including iron and PM losses.

Fig. 12: Block diagram of CCG model including iron and PM losses.

Fig. 13: Iron and PM losses sub-block.

EMF ripple phenomena, resulting in non-sinusoidal phase currents and undulations in the duty cycle waveforms. These effects can be often disregarded for a quick evaluation of the drive performance, but can result crucial for fine calibration of the motor control, especially for sensorless applications and/or for machines with relevant space harmonic content. Therefore, both the dq and $dq\theta$ approaches are maintained in syreDrive, and can be selected by the user depending on the desired accuracy of the simulation.

4.3 Iron and PM losses

The block diagram of the CCG model was upgraded respect to [1] by including the iron loss and PM loss. In particular, these loss terms can be modeled as an equivalent resistance R_{Fe} in parallel to the motor EMF, as depicted in Fig. 11. The value of R_{Fe} varies with the operating point of the machine. Besides the decrease in motor efficiency, these rotational losses have two main effects on the motor modeling: 1) the magnetizing current i_{dq}^m is lower than the phase current i_{dq}; 2) the motor output torque T is lower than the electromagnetic torque T_{em}.

The upgraded CCG motor model accounting for iron and PM losses and the equivalent block diagram are shown in Fig. 12 and 13. The iron losses are modeled using the the Steinmetz formulation, with the eddy-current loss accounted separately, as described in [13]. The hysteresis losses $P_{h,0}$, the eddy currents losses $P_{e,0}$, and the PM losses $P_{PM,0}$ (if any) are evaluated over the entire dq plane and constant pulsation ω_0, and stored in dedicated LUTs. As shown in Fig. 13, the LUTs input is the magnetizing current vector i_{dq}^m provided by the inverse magnetic model. As described in [13], the loss maps are computed at a reference electrical speed ω_0, and their output is scaled based on the instantaneous speed ω according to the Steinmetz equations:

$$P_{Fe} = P_{h,0} \cdot \left(\frac{\omega}{\omega_0}\right)^\alpha + P_{e,0} \cdot \left(\frac{\omega}{\omega_0}\right)^2 \quad (9)$$
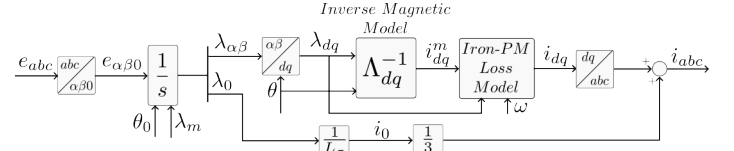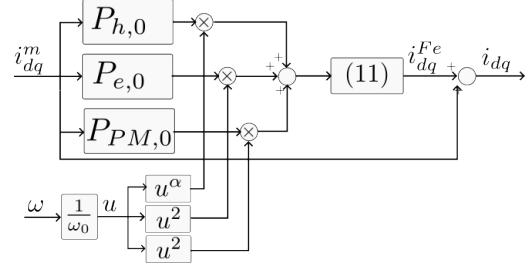
$$P_{PM} = P_{PM,0} \cdot \left(\frac{\omega}{\omega_0}\right)^2 \quad (10)$$

where α is a loss coefficient typical of the selected material. Using the total losses $P_{Fe} + P_{PM}$, the current vector i_{dq}^{Fe} representing the iron and PM losses is obtained as:

$$i_{dq}^{Fe} = conj\left(\frac{2}{3} \cdot \frac{P_{Fe} + P_{PM}}{j \cdot \omega \cdot \lambda_{dq}}\right) \quad (11)$$

Finally, the i_{dq}^{Fe} vector is added to i_{dq}^m, obtaining the total phase current vector i_{dq}. This is transformed to abc frame and fed to the CCGs generators.

The effects of the implemented losses on the i_{dq} current and torque are highlighted in Fig.14, where the same PMSM motor used for the $dq/dq\theta$ comparison is operating using a FOC current control at 10000 rpm. It can be noted that when the iron and PM losses are neglected, the i_{dq} currents follow their reference i_{dq}^*. On the other side, when losses are taken into account, a noticeable reduction in the i_q current is present, resulting in a lower motor torque due to the iron and PM losses effect.

As expected, the implementation of the iron and PM losses in the simulation causes slightly higher computational burden. Moreover, the accuracy of these maps is not always guaranteed by FEA softwares, and these are difficult to be determined by experiments. For these reasons, also the iron and PM losses representation can be either included or not in the syreDrive simulation, based on the user settings.
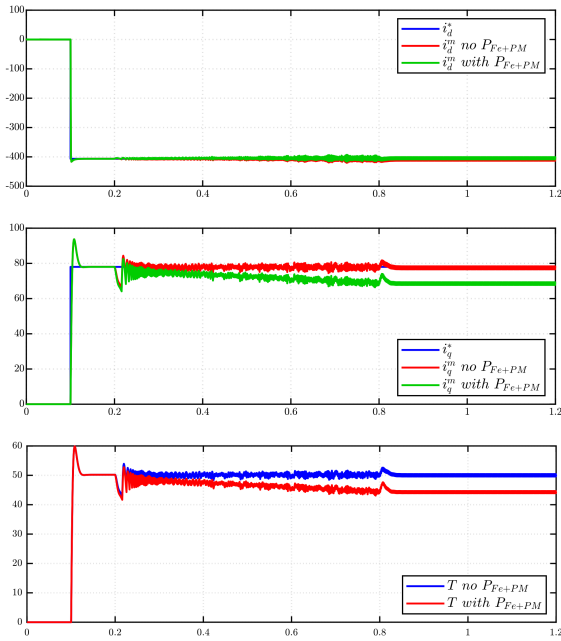
Fig. 14: Effect of iron and PM losses on the i_d and i_q currents and electromagnetic torque T_{em}.

5 Experimental validation

An automotive PMSM, rated 70 kW, 130 Nm and 4200 rpm was experimentally characterized and tested, to validate the proposed motor model. The machine under test (MUT) is controlled with FOC using dSPACE 1202 MicroLabBox and it is coupled with a driving machine imposing the shaft speed. A picture of the test rig is presented in Fig.15. The MUT flux maps were experimental measured and implemented in the simulation model. After that, simulated currents were compared with the measured ones, to verify the accuracy of the simulation model in representing the real MUT behaviour. The MUT was tested both in steady state operating condition and during an Active-Short-Circuit (ASC) fault scenario.
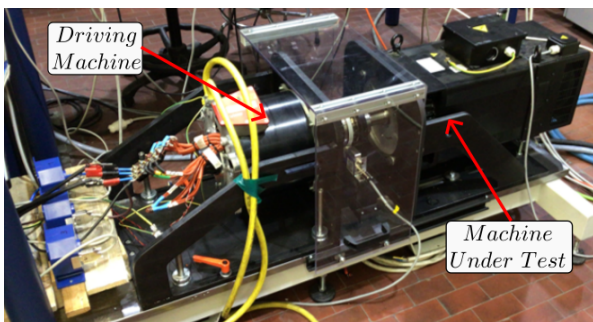

Fig. 15: Test rig used for experimental validation.

5.1 PWM current ripple

The aim of this test was to verify the accuracy of the simulation model in representing the PWM current ripple in steady state conditions. The measured phase current $i_{a,exp}$ is compared with the simulated one i_a at 1000 rpm (in Fig. 16a) and 2000 rpm (Fig. 16b), while commanding the nominal torque. In both tests, the compared waveforms are almost overlapping, demonstrating the high accuracy of the simulation model.
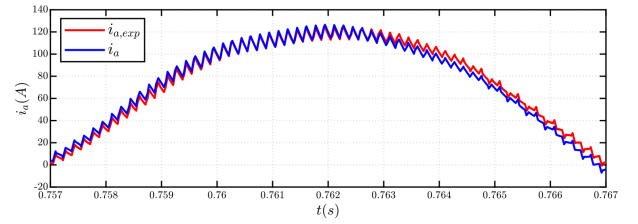

(a)
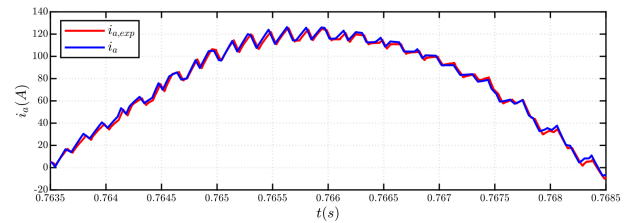
(b)

Fig. 16: Comparison between measured $i_{a,exp}$ and simulated phase current i_a at nominal torque: (a) 1000 rpm and (b) 2000 rpm.

5.2 Active Short Circuit

The MUT was tested under a controlled ASC, by closing the upper switches of the inverter when the driving machine imposes 500 rpm. Before the ASC, the inverter was commanding zero phase current. The experimentally measured current vector $i_{dq,exp}$ is compared with the simulated one i_{dq} in Fig. 17a. It can be noted that the simulation model provides the correct steady state current values and acceptable discrepancy in the transient behaviour. This difference can be explained by a non precise representation in simulation of the driving machine, which speed controller is not immune from the sudden load step due to the ASC. This results in a slight difference between the measured and simulated speed transient, as depicted in Fig.17b. Overall, the e-drive simulation provides satisfying results, confirming that it can be used to study fault conditions.
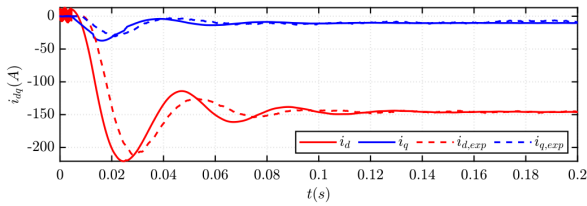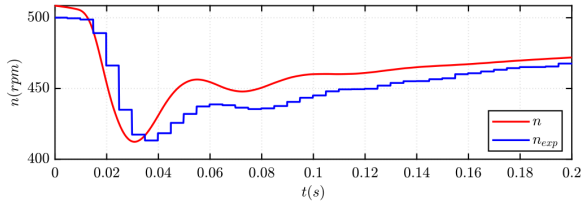
Fig. 17: Results of the ASC test. Comparison between (a) measured $i_{dq,exp}$ and simulated i_{dq} currents and (b) measured and simulated speed.

6 Conclusions

This paper proposes a comprehensive comparison between different simulation approaches for describing synchronous motor drives, either with or without PMs. All the proposed models are implemented both in Matlab-Simulink and PLECS environments, for comparison purposes, and do not require FEA based co-simulation. The circuital models are preferred over the model based ones, as they permit simulating a series of asymmetric fault scenarios. Two types of circuital models are compared, namely VBR and CCG, and the latter one was selected for its lower computational time. The motor model is supplied by a circuital inverter model, which can either set to *instantaneous* or *time average*, if the PWM effects want to be included or not. If desired, the effects of space harmonics can be included as well, moving from the dq to the $dq\theta$ approach, improving the simulation accuracy at the cost of limited additional computational burden. Similarly, if the iron and PM loss maps are known, these can be included in the motor model, to further refine the simulation. The simulation model was validated over the experimental measurements on a commercial traction PMSM, showing accurate results both in healthy and faulty ASC conditions.

The developed simulation model will be included in the syreDrive open source software [1], proposed for combining the motor and control design.

References

[1] A. Varatharajan, D. Brunelli, S. Ferrari, P. Pescetto, and G. Pellegrino, "Syredrive: Automated sensorless control code generation for synchronous reluctance motor drives," in *2021 IEEE Workshop on Electrical Machines Design, Control and Diagnosis (WEMDCD)*, 2021, pp. 192–197.

[2] M. Hinkkanen. "Motulator." (2022), [Online]. Available: https://github.com/Aalto-Electric-Drives/motulator.git.

[3] R. Leuzzi et Al., "Transient overload characteristics of pm-assisted synchronous reluctance machines, including sensorless control feasibility," *IEEE Transactions on Industry Applications*, vol. 55, no. 3, 2019.

[4] J. Pando-Acedo, A. Rassõlkin, A. Lehikoinen, T. Vaimann, A. Kallaste, *et al.*, "Hybrid fea-simulink modelling of permanent magnet assisted synchronous reluctance motor with unbalanced magnet flux," in *2019 IEEE 12th International Symposium on Diagnostics for Electrical Machines, Power Electronics and Drives (SDEMPED)*, 2019, pp. 174–180.

[5] X. Yan and X. He, "Switched reluctance motor driving system simulation based on simulink combined with ansys," in *2010 International Conference on Intelligent Control and Information Processing*, 2010, pp. 744–747.

[6] Mathworks. "Synchronous reluctance machine." (2022), [Online]. Available: https://it.mathworks.com/help/sps/ref/synchronousreluctancemachine.html.

[7] Mathworks. "Fem parameterized pmsm." (2022), [Online]. Available: https://it.mathworks.com/help/sps/ref/femparameterizedpmsm.html.

[8] *Plexim, PLECS User Manual Version 4.6*. 2022, pp. 566–569.

[9] *Plexim, PLECS User Manual Version 4.6*. 2022, pp. 577–580.

[10] L. Wang, J. Jatskevich, and H. W. Dommel, "Reexamination of synchronous machine modeling techniques for electromagnetic transient simulations," *IEEE Transactions on Power Systems*, vol. 22, no. 3, pp. 1221–1230, 2007.

[11] H. Le-Huy and P. Brunelle, "A versatile nonlinear switched reluctance motor model in simulink using realistic and analytical magnetization characteristics," in *31st Annual Conference of IEEE Industrial Electronics Society, 2005. IECON 2005.*, 2005.

[12] S. Ferrari, G. Dilevrano, P. Ragazzo, and G. Pellegrino, "The dq-theta flux map model of synchronous machines," in *2021 IEEE Energy Conversion Congress and Exposition (ECCE)*, 2021, pp. 3716–3723.

[13] S. Ferrari, P. Ragazzo, G. Dilevrano, and G. Pellegrino, "Flux-map based fea evaluation of synchronous machine efficiency maps," in *2021 IEEE Workshop on Electrical Machines Design, Control and Diagnosis (WEMDCD)*, 2021, pp. 76–81.

[14] A. Bojoi. "Advanced dynamic model of e-motor for control rapid prototyping." (Mar. 2022), [Online]. Available: http://webthesis.biblio.polito.it/22088/.

[15] E. Armando, R. I. Bojoi, P. Guglielmi, G. Pellegrino, and M. Pastorelli, "Experimental identification of the magnetic model of synchronous machines," *IEEE Transactions on Industry Applications*, vol. 49, no. 5, pp. 2116–2125, 2013.

[16] S. Zhao, N. Felderer, and J. Allmeling, "Real-time simulation of three-phase current source inverter using sub-cycle averaging method," in *2020 IEEE 21st Workshop on Control and Modeling for Power Electronics (COMPEL)*, 2020, pp. 1–6.